Solid State Ionics 51 (1992) 249–259
North-Holland

SOLID
STATE
IONICS

Three-electrode current–voltage measurements on erbia-stabilized bismuth oxide with sputtered noble metal electrodes

I.C. Vinke, B.A. Boukamp [1], K.J. de Vries and A.J. Burggraaf
Laboratory for Inorganic Chemistry, Materials Science and Catalysis, Department of Chemical Technology, University of Twente, P.O. Box 217, 7500 AE Enschede, The Netherlands

Received 28 June 1991; accepted for publication 28 February 1992

The anodic and cathodic polarization behaviour of sputtered porous gold electrodes on $(Bi_2O_3)_{0.75}(Er_2O_3)_{0.25}$ (abbreviated BE25) was studied as function of temperature and oxygen partial pressure using a three-electrode cell. The anodic polarization is smaller than the cathodic polarization, allowing current densities of 2×10^3 A m^{-2} at 0.1 V and 1041 K in oxygen for oxygen evolution. Comparison with the polarization behaviour of similar sputtered platinum electrodes on BE25 shows little effect of the electrode material on the exchange current densities. This indicates that the electrolyte surface is active in the oxygen transfer process, while the noble metal electrode serves merely as current collector. Analysis of the electrode impedance shows strong influence of surface diffusion on the electrode reaction(s). For the exchange current density an unusual P_{O_2} dependence is observed.

1. Introduction

The stabilized high temperature (defect fluorite) δ-phases of Bi_2O_3 show very high oxygen ion conductivity [1,2]. Of this class of materials bismuth oxide stabilized with 25 mol% erbium oxide, $(Bi_2O_3)_{0.75}(Er_2O_3)_{0.25}$, abbreviated as BE25, has one of the highest conductivities and possesses good mechanical stability down to room temperature [3], although in powdered samples a phase change could be observed [4]. In a previous publication the oxygen pumping characteristics were investigated [5]. In that study it was noted that the cathodic electrode reaction was rate limiting in the total electrode reaction. With increasing sample thickness the limitation of the pumping rates will shift from cathodic rate control to control by the bulk conductivity. It was found that these characteristics were independent of the type of electrode material used (Au and Pt). This is in contrast with what has been found for stabilized zirconia or doped ceria [6,7]. For these electrolytes the platinum electrodes show a much smaller polarization than similar gold electrodes.

If adsorption of oxygen on or diffusion of oxygen over the electrode surface is involved in the rate determining reaction step it is likely that cathodic current limitation will be observed [12,15,16]. In preliminary experiments on BE25 no current limitation was observed within the polarization range of −0.3 to 0.25 V. To investigate the oxygen exchange kinetics on BE25 in more detail the electrode polarization was measured in a three-electrode cell as a function of P_{O_2}, temperature and electrode material. The majority of experiments were performed on BE25 with gold electrodes as gold has a low activity for oxygen adsorption. In this way the activity of the BE25 surface is not masked by the activity of the electrode material. Comparison with "active" platinum can further elucidate the relative influence of the electrode metal.

Impedance measurements were performed as they provide additional insight into the oxygen transfer processes as the electrode/electrolyte interface. Even if a theoretical model predicting the dispersion curve is not available, analysis of the ac-data in terms of an equivalent circuit, composed of electrical analogies of the physical processes, can indicate whether diffusion (Warburg impedance or constant phase

[1] To whom all correspondence should be addressed.

Elsevier Science Publishers B.V.

element (CPE) [8]) or charge transfer reactions (parallel *RC* and/or *RL* circuits [9]) are involved in the rate limiting step(s).

2. Experimental

Ceramic boules of $0.75(Bi_2O_3)$–$0.25(Er_2O_3)$ (BE25) were prepared from powders synthesized by co-precipitation as described by Kruidhof et al. [3]. From the sintered ceramic boules disks were cut of 12 mm Ø and approximately 1.5 mm thickness. These disks were polished with Al_2O_3 using a final grain size of 1 μm. After ultrasonic cleaning an annular gold or platinum electrode of 10 mm outer and 6 mm inner diameter was sputtered on both sides of the disk, see fig. 1. The disks were subsequently annealed at 1123 K for one hour (heating and cooling rate was 1 deg/min). This procedure is needed to relax the stresses introduced in the sample by cutting and polishing and to ensure that the metal electrode has an open structure. The sample was placed in a three-electrode cell [5] in a furnace with controlled atmosphere.

The *I–V* curves were measured using a stepwise increase (or decrease) of the potential, as has been described previously [5]. The corresponding current value was measured after waiting a sufficiently long time to ensure steady state conditions. After each current–voltage experiment an impedance measurement was performed to establish the non-faradaic resistance between the reference and the work electrode.

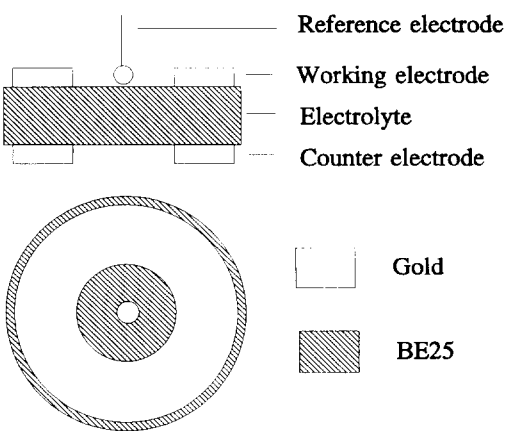

Fig. 1. Electrode configuration used in the three-electrode current–voltage measurements.

3. Results

3.1. Polarization measurements on sputtered gold electrodes

Three-electrode current–voltage curves for BE25 with sputtered gold electrodes, measured in air at various temperatures, are given in fig. 2. At temperatures below about 725 K the *I–V* curves showed hysteresis even under steady state conditions. The magnitude of the hysteresis depends on the *maximum* value of the applied *anodic* polarization. However only the decreasing branch of the *I–V* curve (i.e. going from the maximum anodic to the cathodic polarization) is affected. The *I–V* curve recorded for the cathodic to anodic sweep remained unchanged [10]. As this latter segment still follows a Butler–Volmer type curve its data were used in the analysis.

Fig. 2 shows that high anodic current densities can be obtained at low overpotentials (e.g. for BE25/Au_{sput}: 2.0×10^3 A/m^2 at 0.1 V and 1041 K, as compared to YSZ/Au_{sput}: 8.4×10^{-1} A/m^2 at 0.1 V and

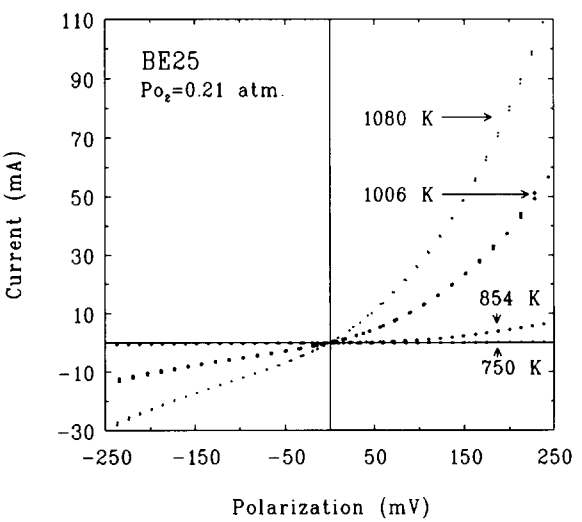

Fig. 2. Examples of *I–V* curves for BE25/$Au_{sputtered}$. The geometrical electrode area is 0.50 cm^2.

1036 K, both in oxygen), indicating fast oxygen release from the electrolyte/electrode combination. The cathodic polarization is larger than the anodic polarization and thus will be the rate limiting step determining the oxygen pumping rate of a symmetric Au/BE25/Au cell as shown previously [5]. It is important to note that, in the polarization range studied, no current limitation is observed.

Tafel-plots of the current–voltage curves yielded estimated values for the oxygen exchange current (i'_O) and the anodic and cathodic charge transfer coefficients (α_a, α_c). Refinement of these parameters in terms of a Butler–Volmer equation with a nonlinear least squares (NLLS) computer program [11] gave reliable fits to the measured I–V curves. The results of the analysis are interpreted as apparent values for i'_O and α'_a and α'_c as these may have been influenced by diffusional processes. The apparent character is denoted by the prime.

The correction for the non-faradiac potential drop, $R_{u(nknown)}$, was also entered as an adjustable parameter in the NLLS procedure. This parameter is essential for obtaining the actual electrode polarization, η, from the applied potential, V. The resulting values for R_u agree well with those obtained from three-electrode impedance measurements, see fig. 3. Hence the inclusion of R_u as a fit parameter gives consistent results.

The apparent exchange current densities (i'_O) show Arrhenius behaviour for all P_{O_2} values (fig. 4). The activation enthalpy, however, changes from 121 kJ/mol at $P_{O_2}=0.01$ atm to 157 kJ/mol at $P_{O_2}=1.0$ atm. A phenomenological relation between current density and P_{O_2} can be expressed by:

$$i_O(T, P_{O_2}) = K_0 \exp\left(\frac{-\Delta H}{RT}\right) \cdot (P_{O_2})^{n(T)} . \qquad (1)$$

The change in activation enthalpies of the Arrhenius plots causes the value of the exponent (n) to change from $n=\frac{1}{2}$ at temperatures around 1000 K to $n=\frac{1}{8}$ at temperatures around 650 K. At high temperatures also a $P_{O_2}^{1/2}$ dependence was observed for $1/R_{el}$ ($\approx i'_O$) for erbia-stabilized bismuth oxides with sputtered platinum electrodes [12].

The temperature dependence of the apparent anodic (α'^{6}_a) and cathodic (α'_c) charge transfer coefficients and of the sum of the apparent coefficients as a function of temperature are shown in fig. 5. For the discussion of the oxygen transfer mechanism the

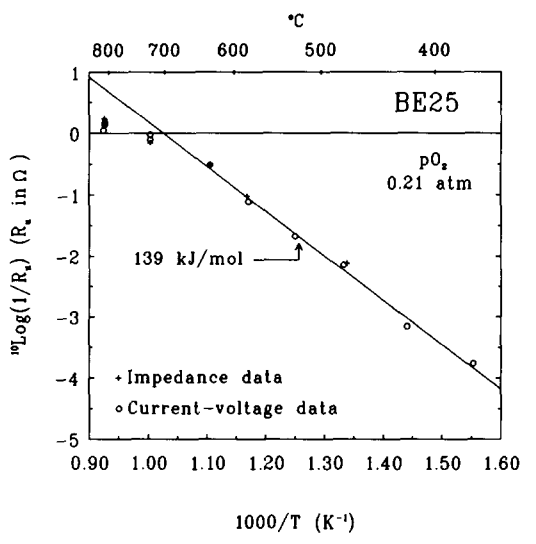

Fig. 3. Comparison of $R_{u(nknown)}$ values obtained from impedance analysis and from I–V curve analysis.

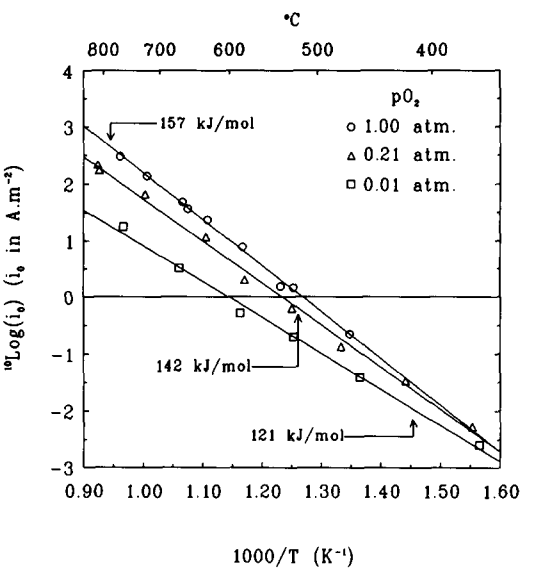

Fig. 4. Arrhenius plot of the apparent exchange current densities for BE25/$Au_{sputtered}$ at three different P_{O_2} values.

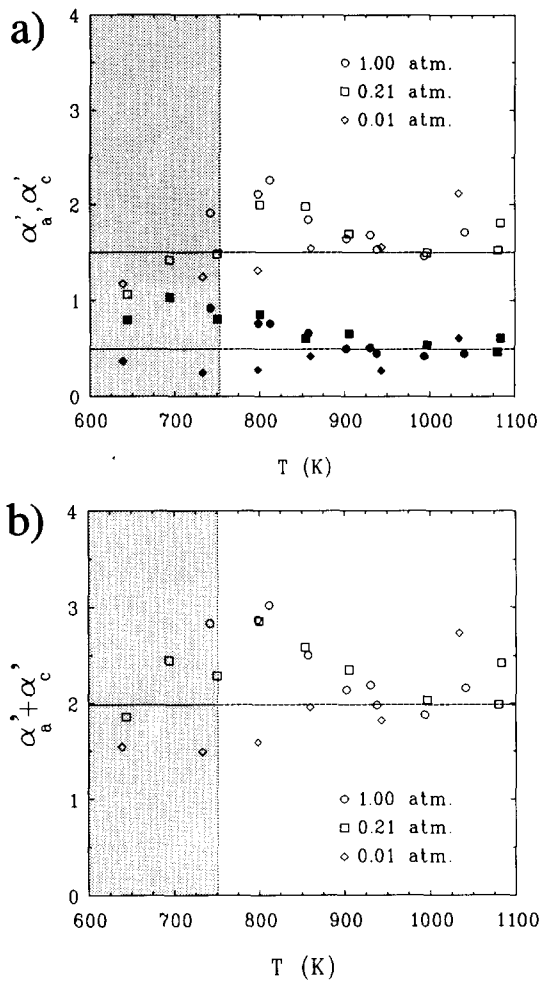

Fig. 5. (a) Variation with temperature of the apparent charge transfer coefficients for $BE25/Au_{sputtered}$ (α'_a open, α'_c closed symbols); (b) sum of the apparent charge transfer coefficients. The shaded area indicates the temperature range where hysteresis occurs. These points are not included in the discussion.

data in the temperature range below 725 K (shaded area in fig. 5) are excluded as the observed hysteresis may effect the α values.

The α'_c values vary only little with temperature and are close to 0.5. The α'_a values show a larger scatter but tend to a value of 1.5 at elevated temperatures.

3.2. Impedance measurements on sputtered gold electrodes

In fig. 6 a few representative impedance spectra are shown for the BE25/sputtered gold system. Analysis of the impedance data was performed with the NLLS-Fit/simulation program "EQUIVALENT CIRCUIT" [13]. For the equivalent circuits and their elements the symbolic notation as described in [13] is used here. Although not always obvious at first sight, the analysis showed that at least two dispersive elements must be present. Of the possible equivalent circuits, the circuit of fig. 7 significantly gave the best fit results. Here Q_i is the symbolic representation of the ith CPE (constant phase element), which is represented in admittance form by [13]:

$$Y^*_Q(\omega) = Y_0(j\omega)^n . \qquad (2)$$

For interfacial impedances it is assumed that CPE behaviour is linked to interface/surface roughness [14].

The simulated dispersions are also shown in fig. 6. The numerical results of the impedance analysis for the entire temperature range in air are given in table 1. R_0 is identical to the non-faradaic resistance R_u (see fig. 2). As expected, R_0 is virtually independent of the P_{O_2}. The elements $(R_1Q_1)(R_2Q_2)$ represent the electrode dispersion. The equivalent circuit suggests that two serial processes are involved in the electrode reaction. At higher temperatures the frequency domains in which the dispersion for the subcircuits (R_1Q_1) and (R_2Q_2) are observed show large overlap. Consequently it is difficult to accurately establish the values for the CPE exponent n (eq. (2)). At temperatures above 750 K the exponent n_2 scatters around 0.5. Hence this CPE then closely resembles a semi-infinite diffusion admittance (Warburg). The deviations from the $\sqrt{\omega}$ dispersion relation may be attributed to surface/interface roughness.

At temperatures below 750 K, R_2 (the dc intercept with the real axis) could not be established from the impedance data as the dispersion associated with the (R_2Q_2) sub-circuit shifts to frequencies below the measurements frequency domain. The parameter values for Q_2, however, could be obtained.

3.3. Polarization measurements on sputtered platinum electrodes

Fig. 8 shows an example of an I–V measurement for BE25 with platinum electrodes in air at 900 K.

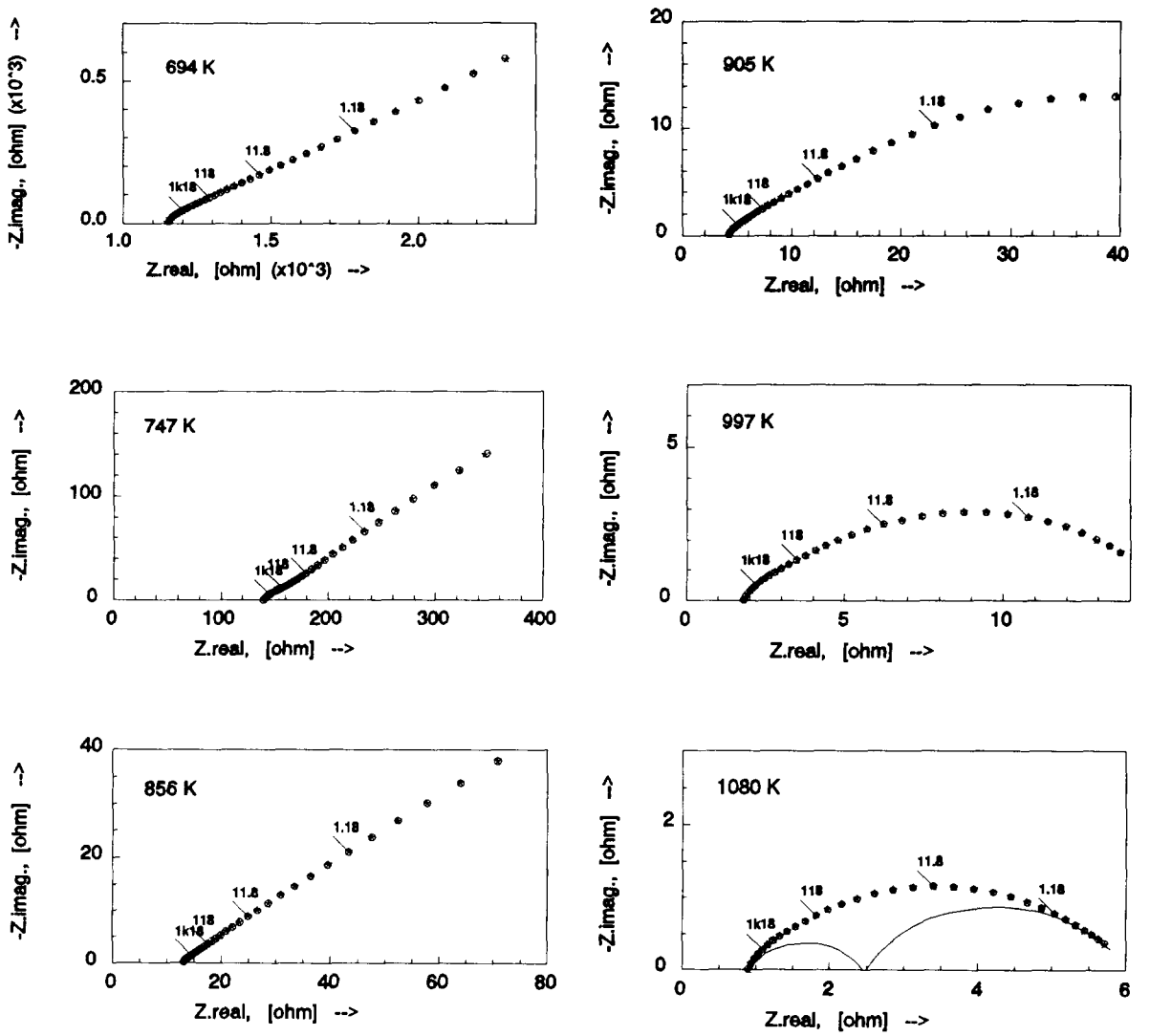

Fig. 6. Impedance diagrams for the BE25/$Au_{sputtered}$ electrode measured in air: (★) measured data points, (○) results from NLLSF-analysis). Frequencies are in Hz. Drawn lines represent the contributions to the dispersion of the separate sub-circuits.

A comparison with fig. 2 (BE25/Au) shows that the general shape of the I–V curves is similar and largely independent of the electrode material. The I–V curves for BE25 with sputtered platinum electrodes can also be analyzed in terms of a Butler–Volmer equation. Fig. 9 provides a comparison between the i'_O values of BE25 with gold or platinum electrodes in air, showing little differences between the two materials. This is remarkable as comparison of the i'_O values for gold and platinum electrodes on YSZ showed differences of up to two orders of magnitude [7].

The choice of electrode material does however influence the oxygen transfer rate under current carrying conditions especially in the anodic regime. This is reflected by the apparent charge transfer coefficients. As in the case for sputtered gold electrodes we do not consider the data analysis for the low temperature measurements (shaded area in fig. 9). Fig. 9 shows the comparison of the α' values. For temperatures above 750–800 K the α'_c values for both

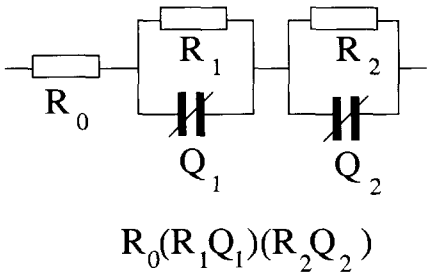

Fig. 7. Equivalent circuit and its symbolic representation [13] used for the NLLSF-analysis of the BE25/$Cu_{sputtered}$ electrode system.

gold and platinum scatter around 0.5 suggesting similar cathodic reactions for both electrode materials. The differences in α'_c values are small. In combination with the identical i'_O values this will lead to similar pumping behaviour for BE25 with gold or platinum electrodes in this temperature region [5].

Comparison of the apparent anodic charge transfer coefficients for gold and platinum (fig. 10) shows that the values of α'_a for platinum at temperatures above 750K seem constant around 1.0. This is in contrast with the values for gold which tend to 1.5 above 750 K as was noted before.

Fig. 10 also gives the sum of the α'_a and α'_c for both gold and platinum electrodes. The values for platinum are close to 1.5 for temperatures above 800 K.

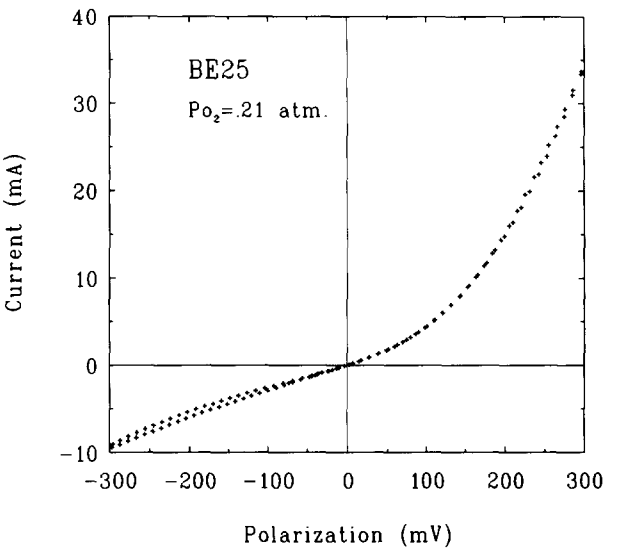

Fig. 8. Example of an I–V curve for BE25/$Pt_{sputtered}$ (T=900 K). The geometrical electrode area is 0.50cm^2.

3.4. Electrode morphology of sputtered electrodes

For a comparison of the properties of the gold and the platinum electrodes the electrode morphology must be well characterized. Fig. 11 presents typical SEM micrographs of a platinum and a gold electrode. The important parameters are the length of the three-phase boundary, the electrolyte/electrode contact surface area, the electrolyte/gas contact surface area and the electrode/gas contact surface area.

Table 1
Parameter values for the elements of the equivalent circuit of fig. 7 as function of temperature (measured in air).

T (K)	R_0 (Ω)	R_1 (Ω)	Q_1 ($\Omega^{-1}S^{n1}$)	n_1	R_2 (Ω)	Q_2 ($\Omega^{-1}s^{n2}$)	n_2
620	6900	1020	3.7×10^{-6}	0.74		2.3×10^{-4}	0.44
644	5400	300	1.6×10^{-6}	0.90		2.6×10^{-4}	0.37
694	1080	260	1.0×10^{-6}	0.96		7.5×10^{-4}	0.28
747	135	7.8	2.6×10^{-4}	0.68		4.0×10^{-3}	0.40
747	132	230	1.9×10^{-3}	0.37	1700	3.7×10^{-3}	0.46
800	43	220	2.0×10^{-2}	0.19		9.0×10^{-3}	0.35
856	10.5	2.3	2.6×10^{-3}	0.40	700	1.1×10^{-2}	0.40
905	3.4	31	1.7×10^{-2}	0.38	30	3.1×10^{-2}	0.64
997	1.4	6.0	2.8×10^{-2}	0.43	8.0	2.4×10^{-2}	0.61
1081	0.57	1.6	5.9×10^{-2}	0.33	3.4	1.6×10^{-2}	0.58

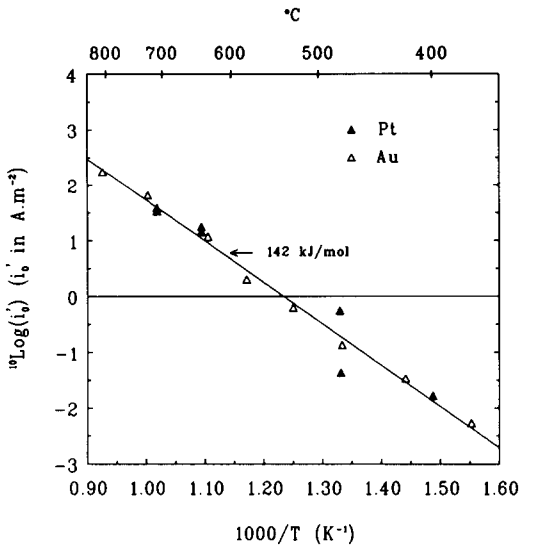

Fig. 9. Comparison of the apparent exchange current densities for BE25 with sputtered gold and with sputtered platinum electrodes, both in air.

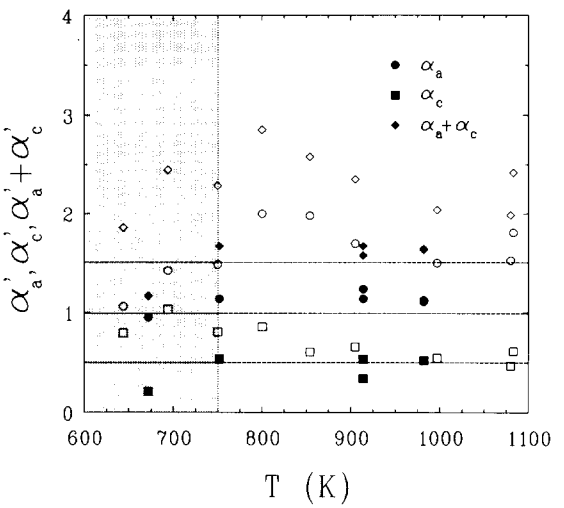

Fig. 10. Comparison of the charge transfer coefficients for BE25 with sputtered gold (open symbols) and with platinum (closed symbols) electrodes. The shaded area indicates the temperature range where hysteresis occurs. These points are not included in the discussion.

In table 2 these estimated values are given per unit total area. The three-phase boundary for the platinum electrode is 8 to 9 times larger than for the gold electrode. The electrolyte area directly exposed to the ambient is approximately two times larger than for the gold electrode, while the electrodes areas exposed to the ambient (including the side walls of the pores) are about equal.

4. Discussion

For the electrochemical exchange reaction of oxygen on the noble metal electrode/oxygen conducting electrolyte system a number of models have been derived [7,12,15–17]. In general these models can be devided into two groups. The first group of models considers the (dissociative) adsorption of oxygen on the electrode metal surface followed by diffusion of oxygen species towards the three-phase boundary where the charge transfer reaction takes place. Verkerk et al. [12] and Nagamoto and Inoue [15] show that for this model current limitation can occur with the following general current voltage relation:

$$I=\rho i_O(\theta_p)\,[\exp(\alpha_a V^*)-\exp(-\alpha_c V^*)] \times\{1+\rho i_O(\theta_p)\gamma[\sqrt{KP_{O_2}}\exp(\alpha_a V^*) +\exp(-\alpha_c V^*)]\}^{-1}, \quad (3)$$

where ρ=length of three-phase boundary/unit area, γ=proportionality constant, K=adsorption equilibrium constant and $V^*=\eta F/RT$, where η is the electrode polarization. θ_p is the equilibrium oxygen partial coverage based on a Langmuir isotherm adsorption model. As the apparent i_O' is strongly dependent on θ_p and the length of the three-phase boundary per unit area it would predict a significant difference between the i_O's for the platinum and the gold electrodes as more oxygen is adsorbed on platinum than on gold (i.e. 1.3×10^{18} at. m^{-2} on Pt [12,18] versus 3.3×10^{16} at. m^{-2} on Au [19] at 1073K and in 1 atm oxygen, both values calculated from the reference literature), while the three-phase boundary for platinum is almost 10 times larger than for gold (table 2).

Mizusaki [16] assumed in his model the charge transfer reaction to be very rapid, and ignored it in his derivation of the current–voltage relation. For both the adsorption and the diffusion limiting case it can be shown that in this model current limitation will occur at rather small polarization values ($\sim$0.1 V). The predicted current–voltage relation is quite different from the typical Butler–Volmer form ob-

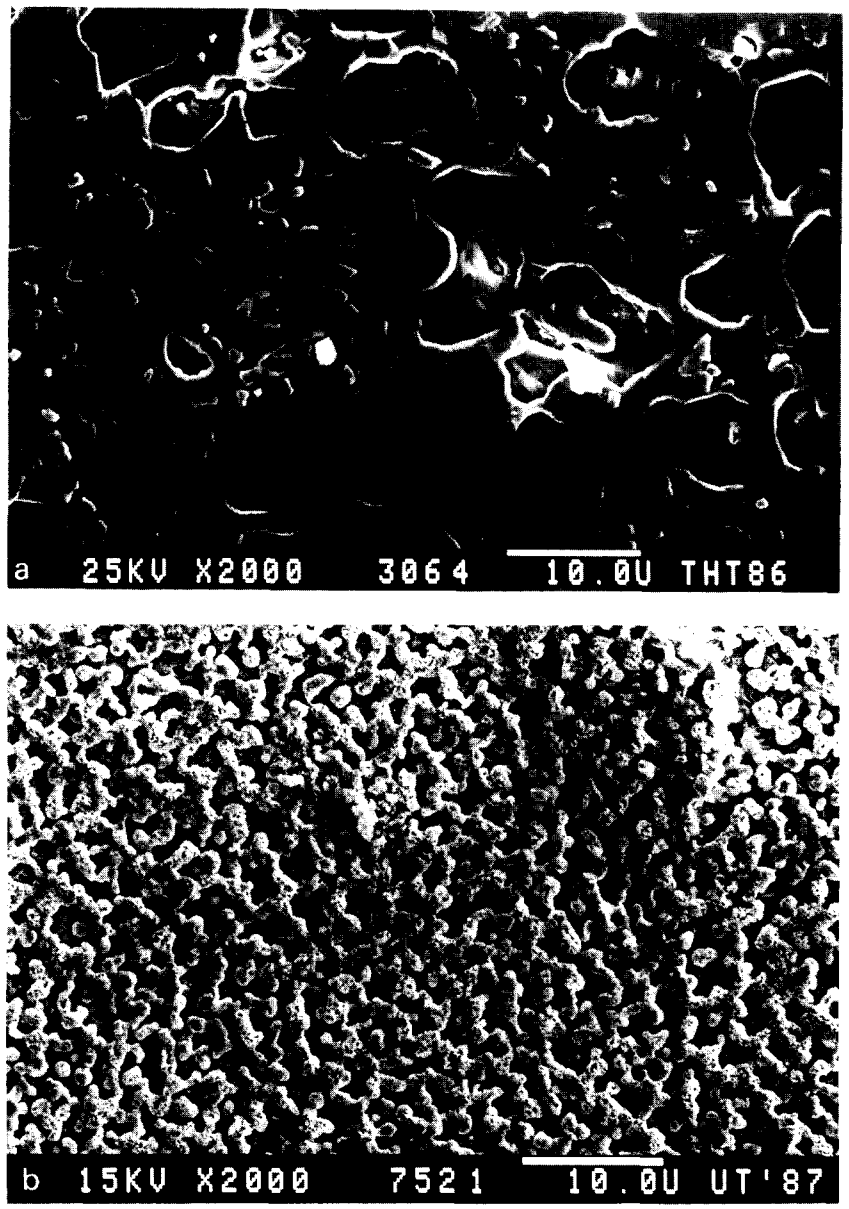

Fig. 11. Electron micrographs of sputtered gold (top) and platinum (bottom) electrodes on BE25.

served in this study. Together with the observations above it must be concluded that adsorption on the electrode cannot be the rate limiting step in the electrode reaction mechanism for the BE25/noble metal system.

As the assumption of a charge transfer reaction limited to a very small region at the three-phase boundary leads locally to unrealistically high current densities Wang and Nowick [7] developed a different model in which the charge transfer reaction takes place in the two-dimensional interface region between the electrode and electrolyte. Oxygen diffuses from the three-phase boundary towards the reaction sites. In this model three limiting cases may be dis-

Table 2
Characteristic data on the morphology of sputtered gold and platinum electrodes on BE25.

Electrode metal	Three-phase line (m/m^2)	Electrolyte/electrode contact surface (m^2/m^2)	Electrolyte/gas contact surface (m^2/m^2)	Electrode/gas contact surface (m^2/m^2)
Pt [12]	1.2×10^6	0.64	0.36	0.80
Au	1.4×10^5	0.83	0.17	0.86
ratio	8.57	0.77	2.12	0.93

cerned: (i) limitation by the rate of (dissociative) adsorption of oxygen on the metal electrode; (ii) diffusion limitation in the electrode/electrolyte interface; and (iii) charge transfer limitation. If charge transfer is rate limiting a symmetrical Butler–Volmer type polarization curve will be observed ($\alpha_s=\alpha_c$). For a slow diffusion process along the electrolyte/electrode interface an asymmetric Butler–Volmer relation is obtained with apparent α's, with $\alpha'_a=1.5\ \alpha_a$ and $\alpha'_c=0.5\ \alpha_c$. The apparent exchange current density, i'_O, is then proportional to $(P_{O_2})^{3/8}$ for dissociative adsorption or $(P_{O_2})^{5/8}$ for associative adsorption of oxygen at the three-phase boundary [7]. If diffusion and charge transfer are fast compared to the rate of adsorption/desorption at the three-phase boundary cathodic current limitation will be observed also.

Robertson and Michaels [17] improved the model of Wang and Nowick by including the back diffusion towards the three-phase boundary for the anodic regime. For all three cases similar solutions are obtained, except that for the diffusion limited case the apparent α' values are equal: $\alpha'_a=0.5\ \alpha_a$ and $\alpha'_c=0.5\ \alpha_c$. As mass transport vanishes for $\eta\to0$ all three limiting cases yield the same relation for the inverse dc-electrode resistance:

$$\frac{dI}{d\eta}=R_{el}^{-1}=2k^0C_0(\theta_0(1-\theta_0))^{1/2}\frac{2F}{kT}, \qquad (4)$$

where $k^0=$ an overall rate constant, $C_0=$ concentration of (reaction/)adsorption sites in the two phase region and θ_0 is the equilibrium site occupation factor for oxygen at the three-phase boundary. The dc-electrode resistance is inversely proportional to the exchange current density. Hence for a low coverage of oxygen ($\theta_p\ll1$) a $(P_{O_2})^{0.25}$ dependence for i'_O is expected for dissociative adsorption of oxygen ($\theta_p\div\sqrt{P_{O_2}}$) and a $(P_{O_2})^{0.5}$ for associative adsorption ($\theta_p\div P_{O_2}$). These P_{O_2} dependencies for θ_p follow from the Langmuir adsorption isotherm model.

According to these last two models again a significant difference in i'_O values should be expected as the diffusion length for the platinum electrodes is much smaller than for the gold electrode (see fig. 11), while the three-phase boundary line is almost a factor of 10 larger for platinum (see table 2). Also all models predict a P_{O_2} independent activation energy for the exchange current density, as well as constant (temperature and P_{O_2} independent) transfer coefficients.

From the discussion sofar it will be apparent that none of these models can be applied directly to describe the electrode reaction mechanism for the BE25/noble metal electrode system and hence a different mechanism must be assumed. From recent oxygen isotope exchange measurements on solid BE25 samples [20] it was found that the overall surface oxygen exchange rate, k_s, compares quite well with the electrochemically measured exchange current density, assuming the following simple relationship [21]:

$$i_O=4Fk_s\,. \qquad (5)$$

This strongly supports the idea that the *electrolyte surface* is active in the (dissociative [20]) adsorption of oxygen. As the electrodes will then only serve as current collectors no influence of the type of electrode material will be seen. This was observed for the cathodic regime where $\alpha_{c,Pt}$ and $\alpha_{c,Au}$ were both approximately 0.5. For the anodic regime, however, different values were observed with $\alpha_{a,Pt}\approx1$ and $\alpha_{a,Au}\approx1.5$ for temperatures above ~900 K, indicating that the noble metal may influence the desorption rate of oxygen.

Two general mechanisms may be regarded now, the first assuming (dissociative) adsorption of oxygen on the electrolyte surface followed by surface diffusion to the three-phase boundary region. Again

this would locally lead to rather high current densities and, if surface diffusion would be rate limiting, an influence from the electrode morphology should be observed.

The second mechanism involves the transfer of electrons to the adsorbed species at the electrolyte surface. Recent oxygen isotope exchange experiments on BE25 powders indicate the possible formation of adsorbed O^- species as rate determining step in the exchange process [22]. The diffusion of charged oxygen species towards the three-phase boundary region would then require counter diffusion of electronic charge, i.e. it would require a certain amount of electronic surface conductivity. Recent phase stability studies by Kruidhof et al. on erbia stabilized bismuth oxide [4] and yttria stabilized bismuth oxide [23] indicated a limited range of nonstoichiometry for oxygen. This implies the presence of electronic defects, giving rise to a (small) electronic conductivity. This has been confirmed by oxygen permeation studies on BE25 performed in our laboratory [24].

Indications for surface conductivity have been presented earlier by Verkerk and Burggraaf [25]. Recent preliminary experiments [22] indeed showed the presence of surface conductivity, however, definitive conclusions cannot yet be drawn. The importance of (surface) diffusion limitation is also supported by the results of the impedance measurement analysis presented in this paper. The two semi-infinite diffusion elements may then tentatively be attributed to the diffusion of adsorbed O^- species and of electronic charge carriers on or near the electrolyte surface.

Development of a model for the current polarization relations, based on the proposed general mechanisms including the electrolyte surface, will be part of future research. Due to the complexity these derivations are beyond the scope of this paper.

The values of the exponent of CPE-1 (Q_1) around 750–800 K ($n_1 \approx 0.2$–0.4, see table 1) are unusually low. It might be explained by assuming a "distributed Warburg" but analysis of the Y_0 values shows a clear break in the temperature dependence in this temperature range. It might be possible that CPE-1 at $T < 750$ K belongs to a different process than at $T > 800$ K. Hence in the temperature range 750–800 K both processes may contribute to the overal dispersion. Trying to analyse the frequency dispersion with only two (RQ) sub-circuits instead of three may result in a low value for n_1 and also influence n_2 (see table 1) as the associated time constants are not much different.

Finally the change in values of the α_a's with temperature, as well as the remarkable temperature and P_{O_2} dependence of the exchange current density may indicate a shift from one type of reaction model at high temperature to another type of reaction model at lower temperature, but further investigations are necessary to elucidate this.

5. Conclusions

(i) Adsorption of oxygen on the electrolyte surface and surface diffusion of oxygen over the electrolyte play an important role in the electrode reaction mechanism for BE25 with sputtered electrodes.

(ii) The electrochemical behaviour of BE25 with sputtered gold electrodes cannot be explained in terms of existing electrochemical models presented in literature.

(iii) Electronic conductivity in the surface region of the electrolyte may play a role in the electrode reaction on BE25 with sputtered noble metal electrodes.

Acknowledgement

J.L. Backiewicz is acknowledged for performing part of the electrochemical measurements. The research presented here was supported by the Netherlands Foundation for Chemical Research (SON) with financial aid from the Netherlands Organisation for Scientific Research (NWO).

References

[1] T. Takahashi, H. Iwahara and T. Arao, J. Appl. Electrochem. 5 (1975) 187.

[2] M.J. Verkerk and A.J. Burggraaf, J. Electrochem. Soc. 128 (1981) 75.

[3] H. Kruidhof, K. Seshan, B.C. Lippens Jr., P.J. Gellings and A.J. Burggraaf, Mat. Res. Bull. 22 (1987) 1635.

[4] H. Kruidhof, H.J.M. Bouwmeester, K.J. de Vries, P.J. Gellings and A.J. Burggraaf, Solid State Ionics 50 (1992) 181.
[5] I.C. Vinke, K. Seshan, B.A. Boukamp, K.J. de Vries and A.J. Burggraaf, Solid State Ionics 34 (1989) 235.
[6] H.S. Isaacs and L.J. Olmer, J. Electrochem. Soc. 129 (1982) 436.
[7] D.Y. Wang and A.S. Nowick, J. Electrochem. Soc. 128 (1981) 55.
[8] J. Ross Macdonald, Impedance Spectroscopy (Wiley, New York, 1987).
[9] B.A. van Hassel, Transport and oxygen transfer properties of ion implanted yttria stabilized zirconia, Ph.D. Thesis (University of Twente, 1990).
[10] I.C. Vinke, K. Seshan, B.A. Boukamp, K.J. de Vries and A.J. Burggraaf, Extended abstracts, 38th Meeting Intern. Soc. Electrochem. (Maastricht, 1987) Vol. I, p. 212.
[11] B.A. Boukamp, I.C. Vinke, K. Seshan, K.J. de Vries and A.J. Burggraaf, Solid State Ionics 28–30 (1988) 1187.
[12] M.J. Verkerk, M.W.J. Hammink and A.J. Burggraaf, J. Electrochem. Soc. 130 (1983) 70.
[13] B.A. Boukamp, Solid State Ionics 20 (1986) 31.
[14] J.B. Bates and Y.T. Chu, Solid State Ionics 20 (1986) 31.
[15] H. Nagamoto and H. Inoue, J. Electrochem. Soc. 136 (1989) 2088.
[16] J. Mizusaki, K. Amano, S. Yamaguchi and K. Fueki, Solid State Ionics 22 (1987) 313.
[17] N.L. Robertson and J.N. Michaels, AIChE (Symp. Ser. 254) 83 (1987) 56.
[18] J.L. Gland, B.A. Sexton and G.B. Fisher, Surface Sci. 95 (1980) 587.
[19] W.R. MacDonald and K.E. Hayes, J. Catal. 18 (1970) 115.
[20] B.A. Boukamp, K.J. de Vries and A.J. Burggraaf, in: Non-Stoichiometric Compounds, Surfaces, Grain Boundaries and Structural Defects, eds. J. Nowotny and W. Weppner (Kluwer, Amsterdam, 1989) p. 299.
[21] B.A. Boukamp, I.C. Vinke, K.J. de Vries and A.J. Burggraaf, Solid State Ionics 32/33 (1989) 918.
[22] I.C. Vinke, Electrochemical and electrode properties of stabilized bismuth-oxide ceramics, Ph.D. Thesis (University of Twente, the Netherlands 1991) chapt. 7.
[23] H. Kruidhof, K.J. de Vries and A.J. Burggraaf, Solid State Ionics 37 (1990) 213.
[24] H.J.M. Bouwmeester, H. Kruidhof, A.J. Burggraaf and P.J. Gellings, in: Proc. Third Intern. Symp. on Systems with Fast Ionic Transport, ed. H. Ullmann, Holzhau, Germany , April 1991.
[25] M.J. Verkerk and A.J. Burggraaf, J. Electrochem. Soc. 130 (1983) 78.